Nano Energy 28 (2016) 216–223

Contents lists available at ScienceDirect

Nano Energy

journal homepage: www.elsevier.com/locate/nanoen

Cathodic polarization suppressed sodium-ion full cell with a 3.3 V high-voltage

Wenhao Ren, Xuhui Yao, Chaojiang Niu, Zhiping Zheng, Kangning Zhao, Qinyou An *, Qiulong Wei, Mengyu Yan, Lei Zhang, Liqiang Mai *

State Key Laboratory of Advanced Technology for Materials Synthesis and Processing, Wuhan University of Technology, Wuhan 430070, China

ARTICLE INFO

Article history:
Received 17 June 2016
Received in revised form
19 July 2016
Accepted 3 August 2016
Available online 16 August 2016

Keywords:
High-voltage
$Na_3V_2(PO_4)_3$
Sodium-ion full cell
Polarization suppression

ABSTRACT

The application of sodium-ion batteries (SIBs) is largely depended on the high energy density electrode system since it suffers from intrinsic high voltage of Na (0.33 V *vs.* Li). To overcome these limitations, we propose a high-voltage sodium-ion full cell *via* cathodic polarization suppression. NASICON structured $Na_3V_2(PO_4)_3$ (NVP) cathode and poorly-graphitized hard carbon (HC) anode are synthesized as the targeted materials through an easily scalable coprecipitation method and a simple biomass-directed technique, respectively. Through morphologic optimization and carbon decoration, the NVP half cell demonstrates a high output voltage of 3.4 V, ultralong cyclability (over 4000 cycles) and distinguished rate capability (77 mA h g^{-1} at 150 C), which is attributed to the enhanced electrical transport behaviors and carrier transmission dynamics. When extended to NVP//HC, the overpotential has been successfully restrained, and the full cell exhibits a theoretical average voltage of 3.3 V, which shows substantial increases in the energy density (> 20%) compared to bulk and bare NVP based full cell. The prototype design of high-energy and low-cost sodium-ion full cell in this work opens the door for accelerating the development and application of SIBs.

1. Introduction

Lithium ion batteries (LIBs) have attracted numerous attentions for renewable energy applications due to their high energy density and excellent cycling stability [1–4]. Nevertheless, the limited availability and increasing cost of lithium source can hardly satisfy the worldwide needs for low-cost electrical energy storage. Sodium, another alkali element with similar chemical property to that of lithium, could be used as a substitute to meet the needs of rechargeable batteries due to the abundant resource and low-cost. Intense interest in the use of sodium-ion batteries (SIBs) particularly for large-scale energy storage has recently been lighted up [5–8]. However, the energy density of the SIBs which is extremely important for application has been serious limited due to the intrinsic high potential of Na (0.33 V *vs.* Li) [9,10]. Besides, the insertion of Na ions into the structure is always a demerit owing to the large ionic size (1.02 Å), resulting in higher polarization and decreased discharge voltage of the SIBs. Thus, the design and fabrication of high-voltage electrode system with suppressed polarization is of great importance for the development of high energy density SIBs.

Recently, a series of cathode materials have been investigated for rechargeable SIBs, such as oxides [11–13], polyanionic compounds [14–16], and Prussian blue analogs [17,18]. However, the cycling stability and rate performance remains discontented due to the low chemical reaction kinetics for Na ions insertion. In contrast, the open framework NASICON (Na super-ionic conductor) structure which provides multichannel ionic conduction and large interspaces is of great benefit to the insertion of Na ions [19,20]. Among NASICON structured materials, $Na_3V_2(PO_4)_3$ (NVP) exhibits a flat voltage plateau at 3.4 V and has a relative high reversible capacity (118 mA h g^{-1}), which endows it great potential as the SIBs cathode [21–23]. Yu et al. [14] reported the interconnected 3D tricontinuous NVP/C, which delivered superior rate capability (82 mA h g^{-1} at 100 C) and excellent cycling stability (96% of capacity retention after 2000 cycles). However, the exploration of suitable counter electrode *vs.* NVP to fabricate high-performance sodium-ion full cell still remains unsatisfactory.

Among anode materials, carbonaceous materials are more economically viable and environmental friendly. Several kind of hard carbons (HC) have been reported to have a favorable Na^+ cation storage capacity (250–300 mA h g^{-1}) and good rate capability (up to 10 C) [24–27]. Most importantly, the median voltage of HC is around 0.1 V which further endows it a great potential to be used as a high-energy SIBs anode. Therefore, NVP//HC

* Corresponding authors.
E-mail addresses: anqinyou86@whut.edu.cn (Q. An), mlq518@whut.edu.cn (L. Mai).

http://dx.doi.org/10.1016/j.nanoen.2016.08.010
2211-2855/

electrodes system, which possess a high theoretical operating voltage at 3.3 V, has a great potential to be used as high-energy and low-cost SIBs. Jian et al. [28] initially reported a full cell based on NVP cathode and HC anode. The results show that the average potential of the full cell is 2.7 V and the initial coulombic efficiency is rather low at that moment. Yuan et al. [15] reported a three-dimensional hard carbon based NVP//HC SIBs, and the full cell gives rise to average discharge voltage at 1.6 V. Obviously, the output voltage and energy density of previously reported NVP//HC full cell still remain unsatisfactory and need further systematical optimization.

Herein, we propose a cathodic polarization suppression strategy to fabricate the high-voltage sodium-ion full cell. The NASICON structured $Na_3V_2(PO_4)_3$ cathode and poorly-graphitized hard carbon anode are selected as the targeted materials. Based on coprecipitation and biomass method, scalable synthesized 3D NVP interconnected nanoparticles (NVP-NP) cathode and biomass-derived HC anode are proposed. The electrochemical performances of NVP-NP cathode are drastically promoted through the construction of 3D interconnected framework structure, which provides continuous ion/electron pathways, superior structure integrity, and large electrode–electrolyte contact area. When evaluated as NVP//HC full cell, the polarization has been successfully suppressed through enhanced electrical transport behaviors and carrier transmission dynamics. The NVP//HC shows a theoretical output voltage of 3.3 V and a promoted energy density ($>$ 20%). It is believed that this easily scalable and biomass approach based high-voltage NVP//HC full cell with suppressed polarization can stimulate new way in fabricating high-energy and low-cost SIBs.

2. Experimental section

2.1. Material synthesis

Synthesis of $Na_3V_2(PO_4)_3$/C cathode materials: V_2O_5, $H_2C_2O_4 \cdot 2H_2O$ and NaH_2PO_4 were analytical grade and purchased from the Sinopharm Chemical Reagent Co., Ltd. (Shanghai, China). First, V_2O_5 (1 mmol) and $H_2C_2O_4 \cdot 2H_2O$ (3 mmol) were added in 15 ml water with stirring at 70 °C for 0.5 h to obtain the clear blue solution. Then, NaH_2PO_4 (3 mmol) and glucose (1 mmol) were added and vigorously stirred for 10 min. After that, 50 ml DMF were dropped in above solution and kept stirring for another 10 min. The solution was then dried at 70 °C in air to get the precursor. In the end, the 3D NVP interconnected nanoparticles were obtained after preheating the precursor at 400 °C for 4 h followed by annealing at 750 °C for 8 h in Ar/H_2 (95:5) (5 °C min^{-1}). The detailed schematic diagram of scalable synthesized NVP-NP with V_2O_5 (30 mmol) is shown in Scheme 1 and the weight of final product is above 53 g. For comparison, the NVP-Bulk was prepared without adding DMF, and the NVP-Bare was synthesized without adding DMF, $H_2C_2O_4 \cdot 2H_2O$ and glucose.

Synthesis of hard carbon anode materials: The HC was synthesized through a facile modified biomass method (Fig. 3a). Namely, the collected white internal capsule in the shaddock peel was cut into pieces, extensively washed with deionized (DI) water, and dried at 100 °C overnight in a vacuum oven. The obtained precursor was prepared for the pyrolysis carbonization process (1200 °C for 3 h, heating rate: 5 °C min^{-1}) under an argon atmosphere with the flow rate of 200 sccm min^{-1}. The obtained carbon was carefully washed in a 2 M HCl at 60 °C for 5 h to remove the remaining impurities. Then, the purified samples were further washed with DI water and pure alcohol, and dried at 100 °C overnight in a vacuum oven.

2.2. Materials characterization

XRD measurement was performed to investigate the crystallographic information using a D8 Advance X-ray diffractometer with non-monochromated Cu Kα X-ray source. Field emission scanning electron microscopy (FESEM) images were collected with a JEOL JSM-7100F at an acceleration voltage of 10 kV. TEM and high resolution TEM (HRTEM) images were recorded with a JEM-2100F microscope. Raman spectra was obtained using a Renishaw INVIA micro-Raman spectroscopy system. BET surface areas were measured using Tristar II 3020 instrument by nitrogen adsorption of at 77 K. Carbon content analysis was determined by Vario EL cube CHNSO elemental analyzer.

2.3. Measurement of electrochemical performance

The electrochemical measurements were tested with 2016 coin cells assembled in a glove box filled with pure argon gas. For half cell, sodium metal was used as the anode, a 1 M solution of $NaClO_4$ in ethylene carbon (EC)–dimethyl carbonate (DMC) (1 : 1 w/w) and 5% FEC was used as the electrolyte, and a Whatman glass microfibre filter (Grade GF/F) was used as the separator. The cathode was made by dispersing 70 wt% active material, 20 wt% acetylene black and 10 wt% polyvinylidene fluoride (PVDF) in *N*-methyl pyrrolidone (NMP) with stirring for 0.5 h. The anode was made by dispersing 80 wt% active material, 10 wt% acetylene black and 10 wt% carboxylmethyl cellulose (CMC) in water with stirring for 0.5 h. Then, the cathode/anode slurry was coated uniformly on Al/Cu foil and dried overnight at 70 °C to yield the working electrodes. The battery was aged for 12 h before test to ensure full absorption of the electrolyte into the electrodes. Galvanostatic

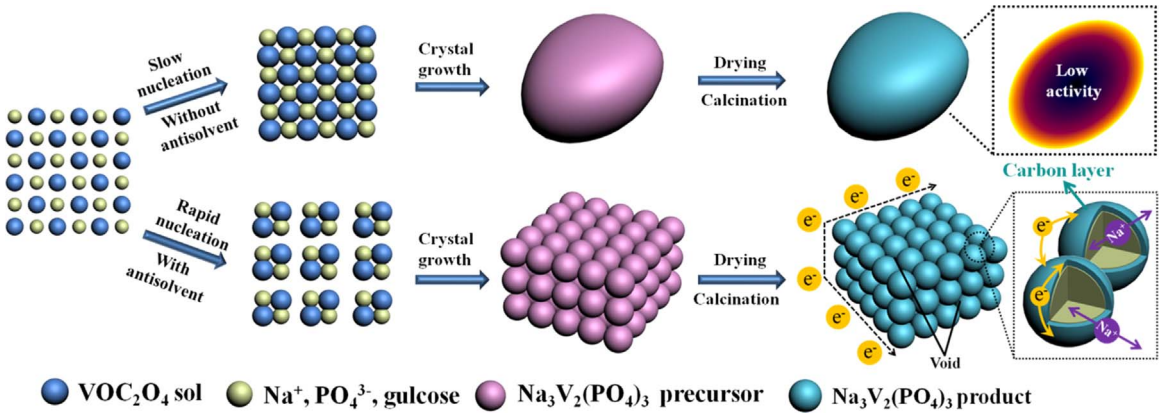

Scheme 1. Schematic diagram of the crystal nucleation, growth and calcination processes during the synthesis of NVP-Bulk and 3D NVP interconnected framework.

charge/discharge measurements were performed with a multi-channel battery testing system (LAND CT2001A). CV and EIS were performed with an electrochemical workstation (Autolab PGSTAT302N).

3. Results and discussion

The detailed morphologies, structures, and electrochemical performance of the prepared NVP cathode were characterized. The formation mechanism of the 3D NVP interconnected nanoparticles were investigated through the schematic illustrations (Scheme 1) accompanied by a mass-production experiment (Fig. S1). First, the uniform transparent blue solution was obtained after fully mixing the raw materials in water bath. Then, with the addition of N,N-Dimethylformamide (DMF) antisolvent, the solubility of solutes have been dramatically decreased, resulting in faster crystal nucleation rate compared with crystal growth rate. Thus, a large amount of small original grain was formed within a short time [29]. Finally, the 3D interconnected nanoparticles framework was constructed owing to the crystal growth process of the grain. For further understanding of antisolvent effect, a control experiment without DMF was carried out. Instead of forming the uniform nanoparticles, the NVP precursor with bulk morphology (NVP-Bulk) was obtained due to the slow nucleation rate, as shown in Fig. S2. Besides, the NVP-Bare was also synthesized without the addition of DMF and carbon sources (Fig. S3). Notably, the whole synthesis process for NVP precursor takes less than 1 h and the enlarged experiments with above 50 g product is easily achieved even in lab-scale. It is safe to draw the conclusion that the co-precipitation strategy presented here is an foolproof way for low-cost and high-production $Na_3V_2(PO_4)_3$ fabrication.

The scanning electron microscopy (SEM) images (Figs. 1a and b) reveal that the nanoparticles are uniformly distributed and the diameter is around 80 nm. The corresponding energy dispersive spectrometry (EDS) element mappings (Fig. S4) show that Na, V, O, P, and C are equably distributed in NVP-NP. The crystal structures of NVP-NP, NVP-Bulk and NVP-Bare were determined through X-ray diffraction (XRD) measurements (Fig. 1c). Both the NVP-NP and NVP-Bulk materials are well indexed to the NASICON structured NVP with a $R\bar{3}c$ space group (JCPDS card no. 00-053-0018), which is in good agreement with previous reports [30,31]. However, the NVP-Bare has two impure peaks at 13° and 34° due to the lack of carbon and partial oxidation during calcinations process [19,21]. The interconnected network structure of NVP-NP is further confirmed by transmission electron microscopy (TEM) image (Fig. 1d). An amorphous carbon shell of around 3 nm can be clearly seen from HRTEM image (Fig. 1e), and the lattice fringes with *d*-spacing of around 6.20 Å correspond to the (012) interplane of rhombohedral NVP. The pore distribution and specific surface area (56.1 $m^2 g^{-1}$) of NVP-NP (Fig. 1f) are determined through Brunauer-Emmett-Teller (BET) test. The main pore-size distribution of NVP-F is around 20 nm, which indicates that the interconnected nanoparticles can create some interspaces and voids for rapid ionic diffusion. In order to study the property of carbon shell, Raman spectrums (Fig. S5) of NVP-NP, NVP-Bulk and NVP-Bare are given. The NVP-Bare exhibits a bands located at 1000 cm^{-1}, corresponding to the Raman fingerprint characteristics of $Na_3V_2(PO_4)_3$ (PO_4^{3-}) [28]. After carbon coating, two characteristic bands located at 1332 cm^{-1} and 1593 cm^{-1} can be assigned to D-band (disorder) and G-band (crystalline graphitized). The peak intensity ratio of I_G/I_D is calculated to be 0.99 and 0.93 for NVP-NP and NVP-Bulk, demonstrating a higher degree of graphitization in NVP-NP. The carbon contents of NVP-NP and NVP-Bulk are 7.93% and 7.97%, respectively, which are characterized by CHNSO elemental analyzer.

The sodium storage behaviors of the NVP-NP, NVP-Bulk and NVP-Bare materials were performed through cyclic voltammetry (CV) analysis (Fig. 2a). All the samples exhibit similar peaks at a scan rate of 0.1 mV s^{-1} in the potential window of 2.5–4.0 V, corresponding to the electrochemical reaction of V^{3+}/V^{4+} [32]. The potential interval between the cathodic and anodic peaks of NVP-NP, NVP-Bulk and NVP-Bare are 166, 225 and 262 mV, respectively, indicating the lower polarization of NVP-NP electrodes. It is obvious that the NVP-NP also exhibits larger curve area and higher redox currents, indicating the higher specific capacity and faster kinetics. Fig. 2b shows the long-term cycling stability of the NVP-NP, NVP-Bulk and NVP-Bare at 15 C (1 C=118 mA g^{-1}). Even

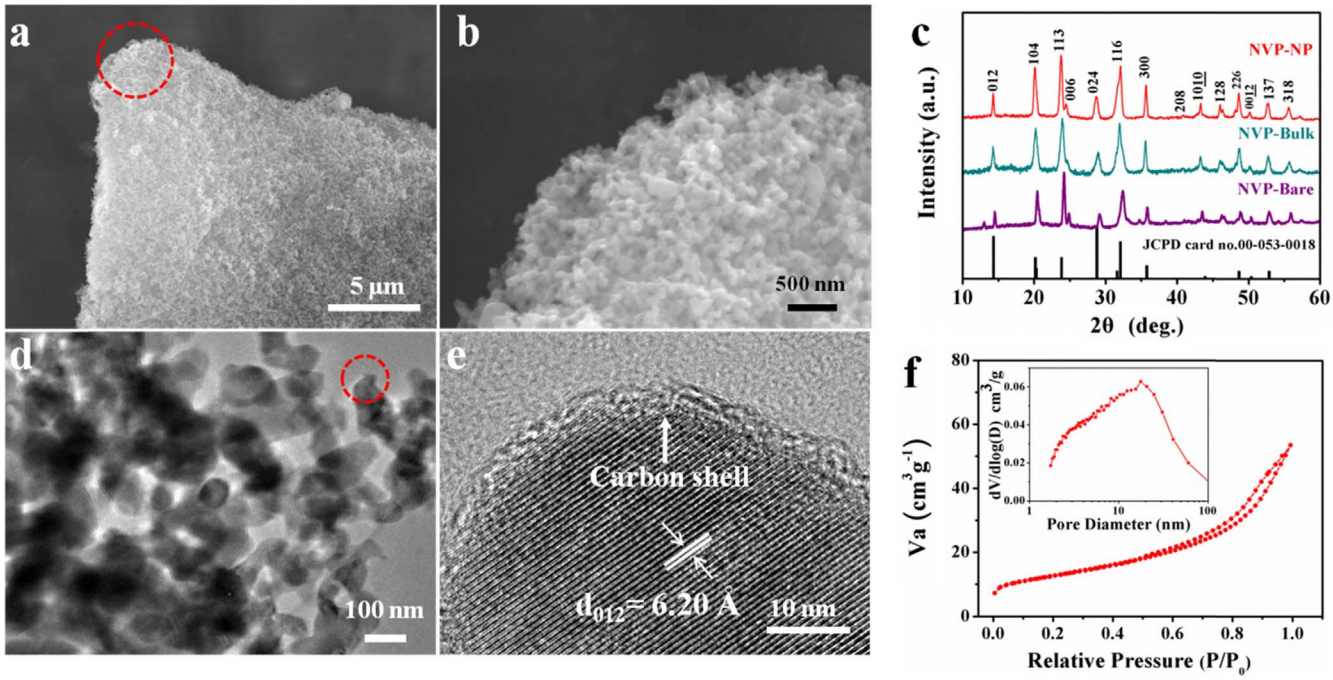

Fig. 1. SEM (a and b) images of NVP-NP. (c) XRD patterns of NVP-NP, NVP-Bulk and NVP-bare. TEM (d and e) images and BET results (f) of NVP-NP.

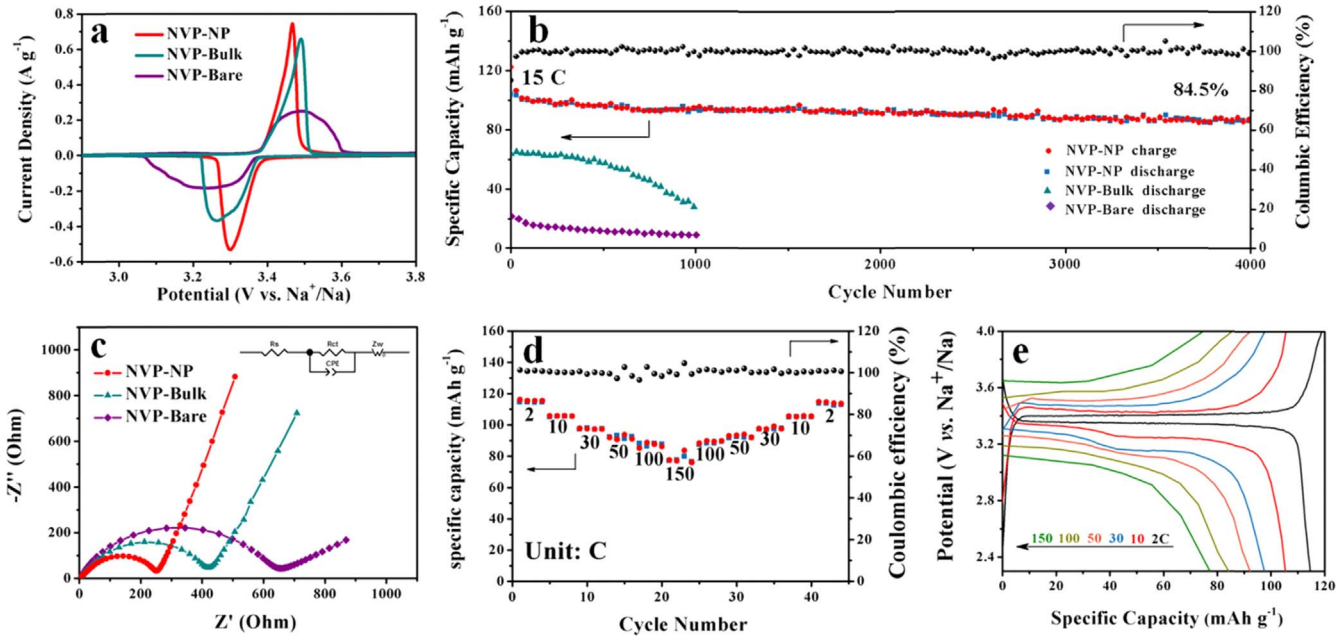

Fig. 2. The electrochemical performance of NVP (*vs.* Na^+/Na): (a) The CV curves of NVP-NP, NVP-Bulk and NVP-Bare at a scan rate 0.1 mV s^{-1}. (b) Cycling performance of NVP-NP, NVP-Bulk and NVP-Bare at the current density of 15 C. (c) EIS spectra of NVP-NP, NVP-Bulk and NVP-Bare after fully charged to 4.0 V. Rate performance (d) and corresponding charge/discharge curves (e) of NVP-NP.

after 4000 cycles, NVP-NP still delivers a specific discharge capacity of 87 mA h g^{-1}, approximately 84.5% of the initial capacity, much better than that of NVP-Bulk and NVP-Bare. Moreover, the coulombic efficiency is stabilized at around 100% throughout cycling, indicating the reversible transport of electrons and ions in the electrodes. The corresponding charge/discharge curves are shown in Fig. S6. The flat voltage plateau is well matched with CV curves and there is no obvious overpotential increase during cycling, manifesting the excellent cycling stability. The detailed reaction kinetics of NVP-NP, NVP-Bulk and NVP-Bare are further investigated by electrochemical impedance spectroscopy (EIS) (Fig. 2c), and the cells are fully sodiated to reach a stable state before the EIS test. It is clear that the charge transfer resistance (R_{ct}) of the NVP-NP (278 Ω) is much smaller than that of NVP-M (426 Ω) and NVP-Bare (638 Ω), demonstrating the improved charge transfer kinetics. Moreover, The straight line at low frequency is attributed to the diffusion of Na ions in the bulk of the electrode material, and the diffusion coefficient value (D) of the Na ions can be calculated using the equation $D=0.5(RT/An^2F^2\sigma_wC)^2$. R is the gas constant, T is the temperature, A is the area of the electrode surface, n is the number of electrons transferred per mole of the active material involved in the electrode reaction, F is the Faraday's constant, σ_w is the Warburg coefficient, and C is the molar concentration of Na ions [30,33]. The apparent Na ion diffusion coefficients for NVP-NP, NVP-Bulk and NVP-Bare based electrodes are calculated to be 4.28×10^{-12}, 3.06×10^{-12} and 1.02×10^{-12} cm^2 s^{-1}, respectively, suggesting the faster sodium diffusion process within the NVP-NP electrode. To evaluate the rate capability, different current densities ranging from 2, 10, 30, 50, 100, to 150 C are performed (Fig. 2d). Notably, even at a high rate of 150 C, the capacity of NVP-NP still remains 78 mA h g^{-1} (67.8% capacity retention). When the current density returns to 2 C, the capacity of NVP-NP can be recovered to 113 mA h g^{-1}, nearly no capacity decay even after suffering from high current density. The corresponding charge/discharge curves (Fig. 2e) show that the overpotential increases followed with the increasing of current density. Remarkably, the discharge voltage plateaus maintain flat at each state even at a high rate of 150 C, demonstrating rapid electron/ion transport. In brief, it is obvious that the NVP-NP possesses enhanced electrical transport behaviors and preferable carrier transmission dynamics compared with NVP-Bulk and NVP-Bare.

The hard carbon was synthesized through a facile biomass method (Fig. 3a) based on previous report [34,35]. Namely, the collected white internal capsule in the shaddock peel was extensively washed, cut into pieces, and sufficiently dried. The obtained precursor was then carbonized and purified to fabricate the final products. The morphology and structure of the HC after annealing and purification are characterized by SEM and TEM. As shown in Fig. 3b, the shaddock peel derived pyrolytic carbon show wrinkled microsheet morphology. The HRTEM images indicate that it has areas of stacked graphite layers with average spacing of about 3.9 Å, as well as amorphous regions (Fig. S7). Fig. 3C shows the XRD pattern of HC-1200, which displays two broad peaks at 24° and 44°, corresponding to the (002) diffraction of the graphitic layer structure and the (101) diffraction of graphite, respectively [34]. Moreover, the Raman spectra (Fig. S8) exhibits two broad bands of the D band at 1335 cm^{-1} (defect-induced band) and G band at 1587 cm^{-1} (crystalline graphitic band). The intensity of the I_G/I_D ratios were 0.92, indicating that the graphene sheets in the materials are highly defective [35].

We further perform CV (0.1 mV s^{-1}) test on HC-1200 electrode in a potential interval of 0.01–2 V (Fig. 3d). Two small reduction peaks at 1.1 and 0.2 V appear only in the first cathodic scan due to the formation of solid electrolyte interface (SEI) and irreversible Na^+ insertion into the bulk material [36,37]. In the following cycles, the CV curves mainly consist two parts, including a pair of sharp redox peaks in the low potential regions and the weak humps at 0.3–1.5 V. The overall sodium storage mechanisms in HC can be attributed to the chemi-sorption on surface heteroatoms [43], metal nanopore filling [36], intercalation between graphene layers [24], and reversible adsorption at structural defect sites in the graphene [44]. Fig. 3e shows the cycling performance of the HC-1200 electrodes at a constant current density of 60 mA g^{-1}. The HC-1200 electrodes exhibit a high discharge capacity of 297 mA h g^{-1} and still maintain a reversible capacity of 264 mA h g^{-1} after 100 cycles, corresponding to 0.11% capacity loss per cycle. Fig. 3f and 3g display the rate performance and its

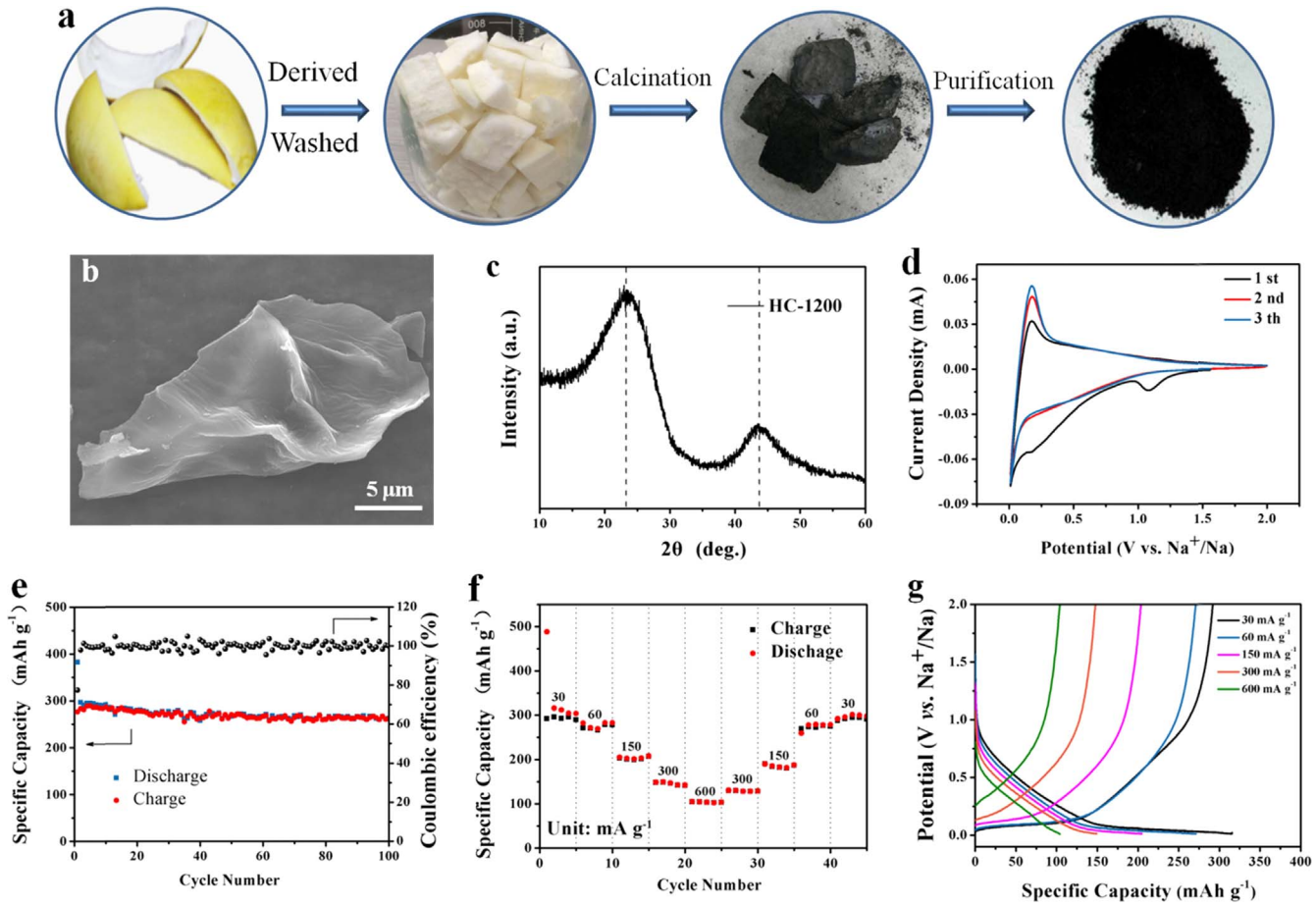

Fig. 3. The characterization of HC anode: (a) Biomass-directed approach for the synthesis of hard carbon. SEM image (b) and XRD pattern (c) of HC-1200. (d) The first three CV curves of HC-1200 at a scan rate 0.1 mV s^{-1}. (e) Cycling performance of HC-1200 at the current density of 60 mA g^{-1}. Rate performance (f) and corresponding charge/discharge curves (g) of HC-1200.

corresponding charge/discharge curves of the HC-1200 electrodes. The electrode delivers reversible capacities of 305, 289, 203, 147 and 104 mA h g^{-1} at the current density of 30, 60, 150, 300, and 600 mA g^{-1}, respectively. When the rate is reset to 30 mA g^{-1} again, the electrode capacity recovers to 300 mA h g^{-1} (98% of the original capacity), which demonstrates the excellent rate capability and superior tolerance of the electrode for rapid Na^+ insertion/extraction.

Through above results, we further assemble the Na ion full cells based on NVP cathode and HC-1200 anode in coin cell. The

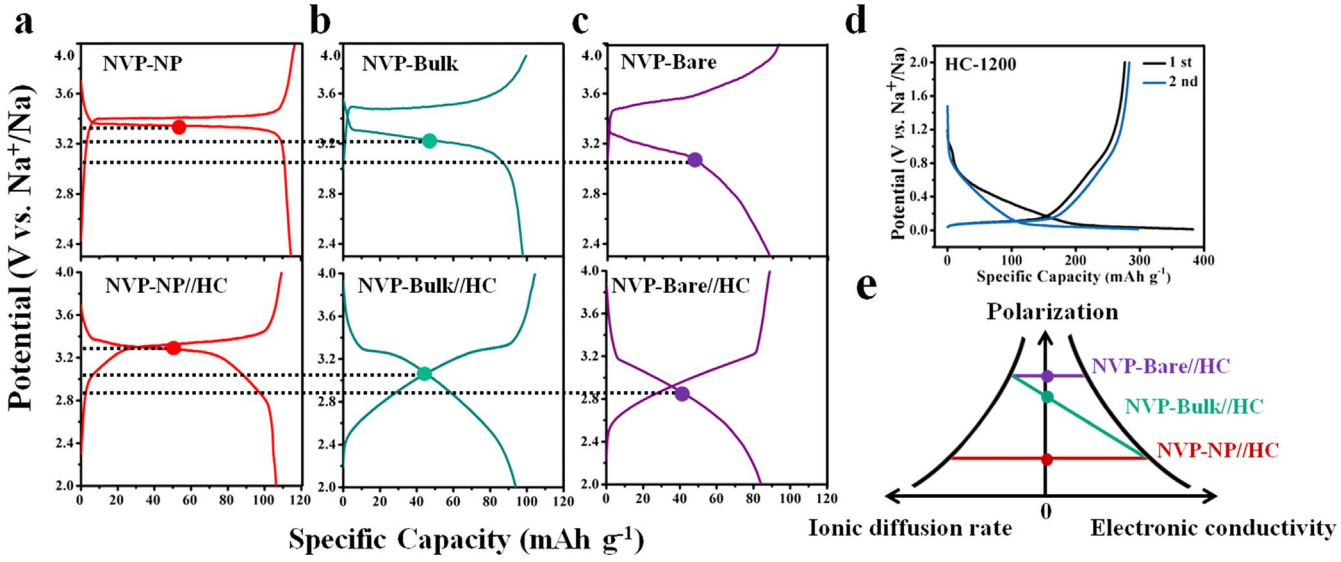

Fig. 4. The second charge/discharge curves of NVP-NP and NVP-NP//HC (a), NVP-Bulk and NVP-Bulk//HC (b), NVP-Bare and NVP-Bare//HC (c) at 0.2 C. (d) The charge/discharge curves of HC-1200 at 60 mA g^{-1}. (e) Schematic illustrations of the relationship among polarization, ionic diffusion rate, and electronic conductivity.

presodiation of the HC-1200 anode is performed prior to cell fabrication (Fig. 4d), and the electrode system balance is achieved by controlling the capacity ratio of cathode/ anode to about 1.05. The detailed assembly of representative full cells with respective to cathode weight are shown in Table S1. Fig. 4a–c display the voltage profiles of the cells for the second charge/discharge under 0.2 C (1 C=118 mA g^{-1}). Obviously, the NVP-NP cathode exhibits the highest output voltage and lowest polarization compared with NVP-Bulk and NVP-Bare, which is in good accordance with the CV (Fig. 2a) and EIS (Fig. 2c) results. The Na ion full cells show the same tendency with half cells, and the NVP-NP//HC demonstrates a median voltage of 3.3 V, which is much higher than that of NVP-Bulk//HC (3.0 V) and NVP-Bare//HC (2.8 V). Compared with NVP-Bulk//HC and NVP-Bare//HC, the specific gravimetric energy of NVP-NP//HC reaches up to 350 W h kg^{-1} based on the mass of cathode (258 W h kg^{-1} based on the mass of both cathode and anode), which shows substantial increases in the energy density (> 20%). It is well known that the proposed overpotential mechanism of the cell can be assigned to the concentration, ohmic and electrochemical polarization. As for the above full cells, the discrepancy is concentrated on the properties of cathode materials including the difference of morphology and conductive carbon decoration. Thus, the high output voltage of the cell is attributed to the 3D interconnected nanoparticles structure of NVP-NP with uniform carbon coating, which provides enhanced ionic diffusion rate and electronic conductivity. The schematic illustrations of the relationship among the polarization, ionic diffusion rate, and electronic conductivity are shown in Fig. 4e. The degree of polarization is followed by a typical Cannikin Law, and the promotion of ionic diffusion rate or electronic conductivity alone doesn't substantially decrease the overpotential of the cell.

The schematic diagram of our NVP//HC full cell is proposed in Fig. 5a. When Na ions is extracted from $Na_3V_2(PO_4)_3$ to form $NaV_2(PO_4)_3$, only Na ions located at Na2 site can be extracted, and the rest of Na ions still remain at Na1 site to maintain the framework structure, resulting in Na2-to-Na2 ionic conduction [31]. Moreover, the cycling performance of the full cells is performed at 0.5 C (Fig. 5b), and it still deliver a discharge capacity of 60 mA h g^{-1} after 100 cycles, which corresponds to 0.43% capacity decay per cycle. To prove the viability of the NVP//HC full cell, the pouch cells are also fabricated. It is clear that the obtained pouch-type battery is capable of lighting the LED bulbs (Fig. 5c). The capacity-potential diagram is applied to display the relationship among discharge capacity, median potential and energy density of sodium-ion full cell based on NVP cathode. Notably, the energy density of our NVP-NP//HC full cell reaches up to 350 W h kg^{-1}, which not only considerably exceeds the performances of previously reported NVP based sodium-ion full cells (Fig. 5d) but also exhibits powerful competitiveness compared with other different categories of rechargeable SIBs (Fig. S9).

Our work offers a facile but effective way to fabricate high-voltage sodium-ion full cell through cathodic polarization suppression. The reasons for the restrained overpotential of NVP-NP based full cell are as follows: (1) The interconnected framework with uniform carbon decoration ensures the fast and continuous electron conduction in the electrode; (2) The 3D structure with pore void is helpful for electrolyte penetration, hence facilitating fast charge transfer across the electrolyte/electrode interface; (3) The 3D interconnected nanoparticles structure offers intimate contact between the carbon layer and NVP nanoparticles, which provides highly conductive matrix for Na ion transport and suppresses the agglomeration of NVP nanoparticles during the Na ion insertion/deinsertion process.

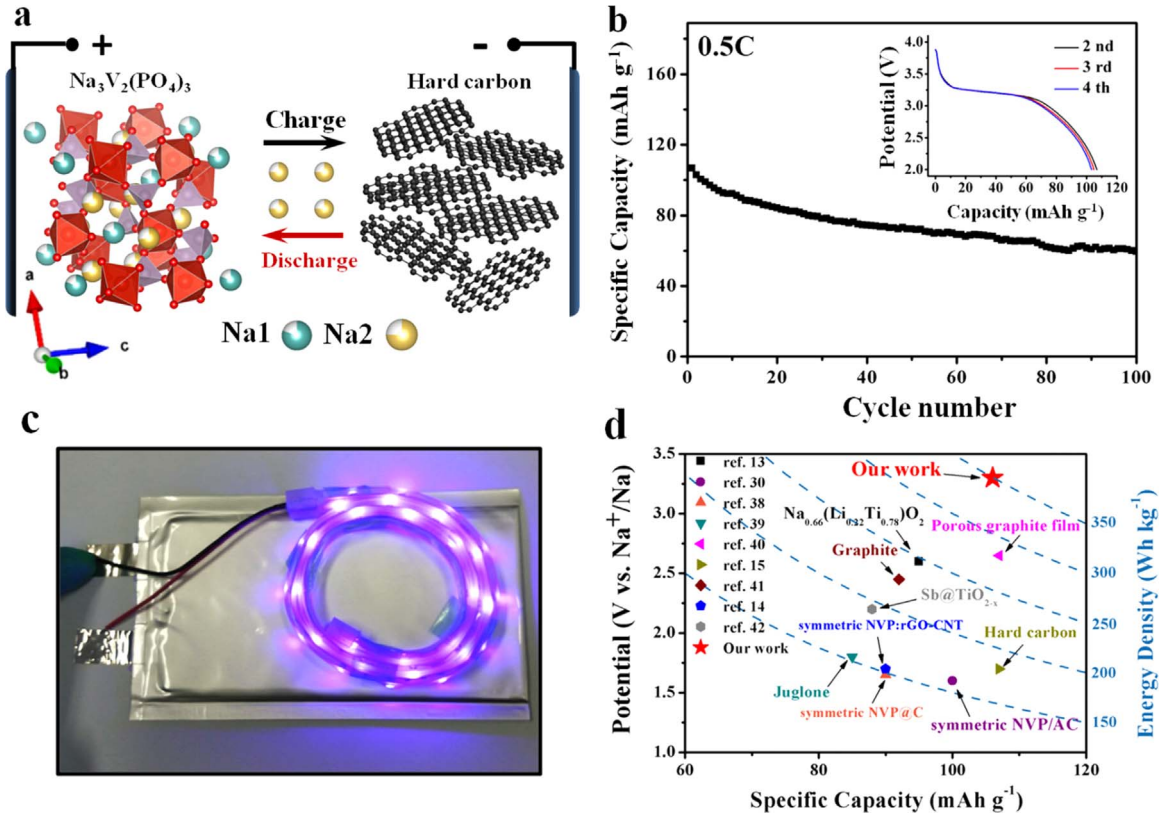

Fig. 5. (a) The schematic diagram of the NVP//HC sodium-ion full cell. (b) The cycling performance of the NVP//HC at 0.5 C. (c) The lighted LED bulbs driven by the flexible pouch cell. (d) The capacity-potential illustrations of the recently published sodium-ion full cells *vs.* $Na_3V_2(PO_4)_3$ as cathode [13–15,30,38–42].

4. Conclusion

In summary, we have developed the cathodic polarization suppressed NVP//HC full cell with a 3.3 V high-voltage based on the easily scalable synthesized 3D interconnected NVP cathode and biomass method fabricated HC anode. The properties of cathode and anode materials have been systematically investigated. Compared with NVP-Bulk and NVP-Bare, the 3D interconnected NVP cathode exhibits a high output voltage of 3.4 V, outstanding cycling stability (84.5% capacity retention over 4000 cycles at 15 C) and superior rate performance (77 mA h g^{-1} at 150 C). Most importantly, the polarization of full cell has been successfully suppressed and the median voltage of NVP-NP//HC reaches up to 3.3 V due to the enhanced electrical transport behaviors and carrier transmission dynamics. The NVP-NP//HC shows substantial increases in the energy density ($>20\%$) towards NVP-Bulk//HC and NVP-Bare//HC, which considerably exceeds the performances of previously reported NVP based sodium-ion full cells and exhibits great potential for renewable energy storage application. This work focuses on not only the development of low-cost cathode/anode materials but also the full-cell design depending on electrochemistry considerations. We believe that this high-voltage NVP//HC full cell with suppressed polarization based on easily scalable and biomass approach can inspire new thought in the construction of high-energy and low-cost rechargeable SIBs.

Acknowledgments

Wenhao Ren and Xuhui Yao contributed equally to this work. This work was supported by the National Basic Research Program of China (2013CB934103 and 2012CB933003), the International Science and Technology Cooperation Program of China (2013DFA50840), the National Natural Science Foundation of China (51302203, 51272197 and 51521001), the Hubei Province Natural Science Fund for Distinguished Young Scholars (2014CFA035), the National Natural Science Fund for Distinguished Young Scholars (51425204), and the Fundamental Research Funds for the Central Universities (WUT: 2015-III-021, 2015-III-032, 2015-III-052 and 2015-PY-2). We are deeply thankful to Professor Dongyuan Zhao of Fudan University for stimulating discussion and kind help.

Appendix A. Supplementary material

Supplementary data associated with this article can be found in the online version at http://dx.doi.org/10.1016/j.nanoen.2016.08.010.

References

[1] Z. Yang, J. Zhang, M.C.W. Kintner-Meyer, X. Lu, D. Choi, J.P. Lemmon, J. Liu, Chem. Rev. 111 (2011) 3577–3613.
[2] S. Xu, Y. Qin, C. Xu, Y. Wei, R. Yang, Z. Wang, Nat. Nanotechnol. 5 (2010) 366–373.
[3] J.B. Goodenough, K.S. Park, J. Am. Chem. Soc. 135 (2013) 1167–1176.
[4] K. Zhao, F. Liu, C. Niu, W. Xu, Y. Dong, L. Zhang, S. Xie, M. Yan, Q. Wei, D. Zhao, L. Mai, Adv. Sci., 2015.
[5] M.H. Han, E. Gonzalo, G. Singh, T. Rojo, Energy Environ. Sci. 8 (2015) 81–102.
[6] S. Kim, D. Seo, X. Ma, G. Ceder, K. Kang, Adv. Energy Mater. 2 (2012) 710–721.
[7] X. Xiang, K. Zhang, J. Chen, Adv. Mater. 27 (2015) 5343–5364.
[8] T. Yang, T. Qian, M. Wang, X. Shen, N. Xu, Z. Sun, C. Yan, Adv. Mater. 28 (2016) 539–545.
[9] N. Yabuuchi, K. Kubota, M. Dahbi, S. Komaba, Chem. Rev. 114 (2014) 11636–11682.
[10] M.S. Islam, C.A. Fisher, Chem. Soc. Rev. 43 (2014) 185–204.
[11] S.M. Oh, S.T. Myung, C.S. Yoon, J. Lu, J. Hassoun, B. Scrosati, K. Amine, Y.K. Sun, Nano Lett. 14 (2014) 1620–1626.
[12] Y. Dong, S. Li, K. Zhao, C. Han, W. Chen, B. Wang, L. Wang, B. Xu, Q. Wei, L. Zhang, X. Xu, L. Mai, Energy Environ. Sci. 8 (2015) 1267–1275.
[13] Y. Wang, X. Yu, S. Xu, J. Bai, R. Xiao, Y.S. Hu, H. Li, X.Q. Yang, L. Chen, X. Huang, Nat. Commun. 4 (2013) 2365.
[14] C. Zhu, P. Kopold, P.A. van Aken, J. Maier, Y. Yu, Adv. Mater. 28 (2016) 2408.
[15] Z. Yuan, L. Si, X. Zhu, J. Mater. Chem. A 3 (2015) 23403–23411.
[16] B. Zhang, R. Dugas, G. Rousse, P. Rozier, A.M. Abakumov, J.-M. Tarascon, Nat. Commun. 7 (2016).
[17] L. Wang, J. Song, R. Qiao, L.A. Wray, M.A. Hossain, Y.D. Chuang, W. Yang, Y. Lu, D. Evans, J.J. Lee, S. Vail, X. Zhao, M. Nishijima, S. Kakimoto, J.B. Goodenough, J. Am. Chem. Soc. 137 (2015) 2548–2554.
[18] J. Song, L. Wang, Y. Lu, J. Liu, B. Guo, P. Xiao, J.J. Lee, X.Q. Yang, G. Henkelman, J. B. Goodenough, J. Am. Chem. Soc. 137 (2015) 2658–2664.
[19] Y. Jiang, Z. Yang, W. Li, L. Zeng, F. Pan, M. Wang, X. Wei, G. Hu, L. Gu, Y. Yu, Adv. Energy Mater. 5 (2015).
[20] Z. Jian, V. Raju, Z. Li, Z. Xing, Y.-S. Hu, X. Ji, Adv. Funct. Mater. 25 (2015) 5778–5785.
[21] C. Zhu, K. Song, P.A. van Aken, J. Maier, Y. Yu, Nano Lett. 14 (2014) 2175–2180.
[22] W. Ren, Z. Zheng, C. Xu, C. Niu, Q. Wei, Q. An, K. Zhao, M. Yan, M. Qin, L. Mai, Nano Energy 25 (2016) 145–153.
[23] Y. Fang, L. Xiao, X. Ai, Y. Cao, H. Yang, Adv. Mater. 27 (2015) 5895–5900.
[24] S. Komaba, W. Murata, T. Ishikawa, N. Yabuuchi, T. Ozeki, T. Nakayama, A. Ogata, K. Gotoh, K. Fujiwara, Adv. Funct. Mater. 21 (2011) 3859–3867.
[25] L. Zhang, K. Zhao, W. Xu, Y. Dong, R. Xia, F. Liu, L. He, Q. Wei, M. Yan, L. Mai, Phys. Chem. Chem. Phys. 17 (2015) 7619–7623.
[26] S. Wenzel, T. Hara, J. Janek, P. Adelhelm, Energy Environ. Sci. 4 (2011) 3342–3345.
[27] K. Zhang, Z. Hu, X. Liu, Z. Tao, J. Chen, Adv. Mater. 27 (2015) 3305–3309.
[28] Z. Jian, W. Han, X. Lu, H. Yang, Y.S. Hu, J. Zhou, Z. Zhou, J. Li, W. Chen, D. Chen, Adv. Energy Mater. 3 (2013) 156–160.
[29] Q. An, F. Xiong, Q. Wei, J. Sheng, L. He, D. Ma, Y. Yao, L. Mai, Adv. Energy Mater. 5 (2015).
[30] S. Li, Y. Dong, L. Xu, X. Xu, L. He, L. Mai, Adv. Mater. 26 (2014) 3545–3553.
[31] Z. Jian, C. Yuan, W. Han, X. Lu, L. Gu, X. Xi, Y.-S. Hu, H. Li, W. Chen, D. Chen, Y. Ikuhara, L. Chen, Adv. Funct. Mater. 24 (2014) 4265–4272.
[32] K. Saravanan, C.W. Mason, A. Rudola, K.H. Wong, P. Balaya, Adv. Energy Mater. 3 (2013) 444–450.
[33] W. Ren, Z. Zheng, Y. Luo, W. Chen, C. Niu, K. Zhao, M. Yan, L. Zhang, J. Meng, L. Mai, J. Mater. Chem. A 3 (2015) 19850–19856.
[34] N. Sun, H. Liu, B. Xu, J. Mater. Chem. A 3 (2015) 20560–20566.
[35] E.M. Lotfabad, J. Ding, K. Cui, A. Kohandehghan, W.P. Kalisvaart, M. Hazelton, D. Mitlin, ACS Nano 8 (2014) 7115–7129.
[36] Y. Cao, L. Xiao, M.L. Sushko, W. Wang, B. Schwenzer, J. Xiao, Z. Nie, L.V. Saraf, Z. Yang, J. Liu, Nano Lett. 12 (2012) 3783–3787.
[37] L. Xiao, Y. Cao, W.A. Henderson, M.L. Sushko, Y. Shao, J. Xiao, W. Wang, M. H. Engelhard, Z. Nie, J. Liu, Nano Energy 19 (2016) 279–288.
[38] W. Duan, Z. Zhu, H. Li, Z. Hu, K. Zhang, F. Cheng, J. Chen, J. Mater. Chem. A 2 (2014) 8668–8675.
[39] H. Wang, P. Hu, J. Yang, G. Gong, L. Guo, X. Chen, Adv. Mater. 27 (2015) 2348–2354.
[40] P. Han, X. Han, J. Yao, Z. Liu, X. Cao, G. Cui, Electrochem. Commun. 61 (2015) 84–88.
[41] Z. Zhu, F. Cheng, Z. Hu, Z. Niu, J. Chen, J. Power Sources 293 (2015) 626–634.
[42] N. Wang, Z. Bai, Y. Qian, J. Yang, *Adv. Mater.* 2016.
[43] Z. Wang, L. Qie, L. Yuan, W. Zhang, X. Hu, Y. Huang, Carbon 55 (2013) 328–334.
[44] R. Mukherjee, A.V. Thomas, D. Datta, E. Singh, J. Li, O. Eksik, V.B. Shenoy, N. Koratkar, Nat. Commun. 5 (2014).

Wenhao Ren received his B.S. degree in Department of Materials Science and Engineering from Wuhan University of Science and Technology in 2012 and he is currently working toward the Ph.D. degree in Material Science at Wuhan University of Technology. His current research involves nanomaterials and devices for energy storage.

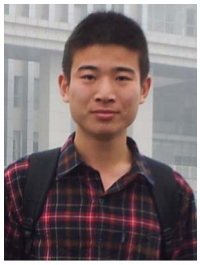

Xuhui Yao received his B.S. degree in Department of Materials Science and Engineering from Wuhan University of Science and Technology in 2016. He has joined WUT-Harvard Joint Nano Key Laboratory for one year. His research is focused on novel nanomaterials for secondary sodium ion batteries.

Chaojiang Niu received his M.S. degree in Material Chemistry from Wuhan University of Technology in 2009. He is currently working toward the Ph.D. degree and his current research focuses on the energy storage materials and devices.

Zhiping Zheng is currently an undergraduate in Wuhan University of Technology. He has learned in WUT-Harvard Joint Nano Key Laboratory for two years under the direct of Professor Mai. His research is focused on synthesis of cathode materials. He shows high interests for fundamental study of materials.

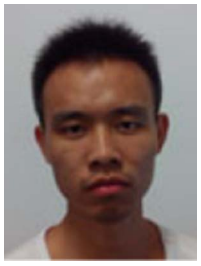

Kangning Zhao received his B.S. degree in Department of Materials Science of Engineering from Wuhan University of Technology in 2012. He has joined WUT-Harvard Joint Nano Key Laboratory for two years. He is currently working toward the Ph.D. degree. His current research involves the nanomaterials achieving high energy density and power density for lithium ion battery and sodium ion battery.

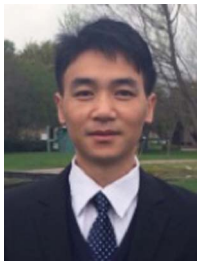

Qinyou An is Associate Professor of Materials Science and Engineering at Wuhan University of Technology (WUT). He received his Ph.D. degree from WUT in 2014. He carried out his postdoctoral research in the laboratory of Prof. Yan Yao at the University of Houston in 2014–2015. Currently, his research interest includes energy storage materials and devices.

Qiulong Wei received his B.S. degree in Department of Materials Science and Engineering from Wuhan University of Technology in 2011. He has joined State Key Laboratory of Advanced Technology for Materials Synthesis and Processing for four years. He is currently working toward the Ph.D. degree. His current research involves the design and synthesis of nanomaterials for achieving both high energy density and power density electrochemical energy storage device, including the lithium-ion battery, sodium ion battery and the hybrid capacitor.

Mengyu Yan received his B.S. degree in Material Chemistry from China University of Geosciences in 2012 and he is currently working toward the Ph.D. degree in Material Science at Wuhan University of Technology. His current research interests include nanoenergy materials and devices.

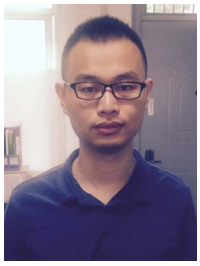

Lei Zhang received his B.S. degree in Department of Materials Science of Engineering from Wuhan University of Technology in 2012. He has joined WUT-Harvard Joint Nano Key Laboratory for four years. He is currently working toward the Ph.D. degree. His current research involves high-energy and high-power density lithium ion batteries.

Liqiang Mai is Chair Professor of Materials Science and Engineering at Wuhan University of Technology (WUT). He received his Ph.D. from WUT in 2004. He carried out his postdoctoral research in the laboratory of Prof. Zhonglin Wang at Georgia Institute of Technology in 2006–2007 and worked as advanced research scholar in the laboratory of Prof. Charles M. Lieber at Harvard University in 2008–2011. His current research interests focus on nanowire materials and devices for energy storage. He is the winner of the National Natural Science Fund for Distinguished Young Scholars, China Youth Science and Technology Award, and Guanghua Engineering Award, and so forth.